Applied Catalysis B: Environmental 148–149 (2014) 114–122

Contents lists available at ScienceDirect

Applied Catalysis B: Environmental

journal homepage: www.elsevier.com/locate/apcatb

Review

Ni-Mn bi-metal oxide catalysts for the low temperature SCR removal of NO with NH_3

Yaping Wan[a], Wenru Zhao[a,*], Yu Tang[a], Liang Li[a], Huijun Wang[a], Yunlong Cui[a], Jinlou Gu[a], Yongsheng Li[a], Jianlin Shi[a,b,*]

[a] Low Dimensional Materials Chemistry Laboratory, School of Materials Science and Engineering, East China University of Science and Technology, 130 Mei long Road, Shanghai, 200237, China
[b] State Key Lab of High Performance Ceramics and Superfine Microstructure, Shanghai Institute of Ceramics, Chinese Academy of Science, 1295 Dingxi Road, Shanghai, 200050, China

ARTICLE INFO

Article history:
Received 2 June 2013
Received in revised form 22 October 2013
Accepted 26 October 2013
Available online 1 November 2013

Keywords:
Low temperature NO-SCR
Nickel and manganese mixed oxides
Surface Mn^{4+} active species
Lewis acid sites

ABSTRACT

A series of nickel–manganese bi-metal oxide catalysts of different Ni/Mn ratios were prepared by a co-precipitation method for the low temperature selective catalytic reduction (SCR) of NO with NH_3 in the presence of excess O_2. The NO conversion over different catalysts decreased in the following sequence of Ni(0.4)-MnO_x > MnO_x » Ni(1)-MnO_x > Ni(2.5)-MnO_x > NiO_x. The Ni(0.4)-MnO_x catalyst showed the highest catalytic activity, 85% of NO conversion at 95 °C and 100% from 120 to 240 °C, among the catalysts investigated. The TPR, XPS, NH_3-TPD and in situ FTIR results revealed that Mn^{4+} was the main active species for SCR reaction and the addition of nickel species enhanced the surface concentration and acidity of Lewis acid sites. A possible synergetic catalytic effect was proposed for the low temperature SCR reaction through the electron transfer between Mn and Ni ions.

Contents

* Corresponding author. Tel.: +86 21 64252599, fax: +86 21 64252599.
E-mail addresses: wenruru@ecust.edu.cn (W. Zhao), jlshi@sunm.shcnc.ac.cn (J. Shi).

0926-3373/$ – see front matter © 2013 Elsevier B.V. All rights reserved.
http://dx.doi.org/10.1016/j.apcatb.2013.10.049

1. Introduction

Nitrogen oxides exhausted from automobiles and industrial combustion of coal and fossil fuel have been leading to a great number of environmental problems including ground level ozone, photo chemical smog and acid rain, and are highly toxic to human health. At present, selective catalytic reduction (SCR) of NO_x with NH_3 in excess O_2 is the most widely used technique for removing of NO_x [1]. V_2O_5-WO_3(MoO_3)/TiO_2 is the typical and efficient commercial catalyst for SCR of NO_x in a relatively high temperature range of 300 °C to 400 °C [2]. To meet the requirement of the high SCR temperature, the SCR reactor should always be located at the upstream of the purification system before particle removal, which, however, brings about the problems such as the deposition of dust on the catalyst and the high expense [3]. Thus the low-temperature (<200 °C) catalysts, which can efficiently work at the downstream after the particle removal where the exhaust gas has cooled down to lower than, e.g., 200 °C, become highly desirable to avoid the above problems.

Recently, manganese-containing catalysts, including MnO_x–TiO_2 [4], Fe-MnO_x/TiO_2 [5], MnO_x [6], Ce-MnO_x [7], Fe-MnO_x [3], Cr-MnO_x [2], and Cu-MnO_x [8,9], have attracted much attention due to their high catalytic activities for the removing of NO_x at low temperature. Pena et al. [10] investigated the low-temperature SCR of NO with NH_3 in the presence of excess O_2 on the oxides of V, Cr, Mn, Fe, Co, Ni and Cu supported on anatase TiO_2 and found the catalytic performance decreased in the following order of Mn > Cu » Cr » Co > Fe » V »> Ni.

A great number of literatures have reported that Mn^{4+} is more preferable than Mn^{2+} and Mn^{3+} for the catalytic reactions over the manganese-containing catalysts. Kapteijn et al. [11] found that the reduction of NO by NH_3 over pure manganese oxides decreased in the order of MnO_2 > Mn_5O_8 > Mn_2O_3 > Mn_3O_4. Tang et al. [12] reported that the catalyst with more Mn^{4+} and richer lattice oxygen showed higher HCHO oxidation activity. Lee et al. [13] found that the oxidation states of manganese in the Mn/TiO_2 catalysts strongly affected their SCR activities at low temperatures and the catalyst with the higher Mn^{4+} content exhibited the better catalytic activity. Yang et al. [3] reported that Mn^{4+} in the $(Fe_{3-x}Mn_x)_{1-\delta}O_4$ catalyst played an important role in the SCR action through both Langmuir–Hinshelwood and Eley–Rideal mechanisms. Thirupathi et al. [1,7] found that the high reducibility and the predominant MnO_2 phase should be responsible for the high SCR activities of the nickel-doped Mn/TiO_2 catalyst.

In this work, a series of Ni-MnO_x mixed oxide catalysts were prepared by ammonium carbonate-assisted co-precipitation of manganese and nickel nitrates [8] with varied molar ratios of Ni/Mn. The activities for the low temperature SCR of NO with NH_3 in the presence of excess O_2 at the relatively high space velocity of 64,000 h^{-1} were investigated. The 400 °C calcined Ni(0.4)-MnO_x catalyst with the molar ratio of Ni/Mn at 1:2.5 exhibited an excellent NO_x SCR performance of complete NO reduction at as low as 150 °C, which can be attributed to the synergetic catalytic effect between Mn and Ni ions, in addition to its relatively high surface area, high surface Mn^{4+} concentration, and the high concentration of Lewis acid sites, as well as, as characterized by BET, XPS, TPR, TPD and in situ FTIR. A synergetic effect based on the electron transfer between nickel and manganese for low-temperature SCR process over the Ni(0.4)-MnO_x catalyst has been proposed.

2. Experimental

2.1. Catalysts preparation

A series of Ni-MnO_x catalysts were prepared by a standard co-precipitation method [8]. A certain amount of nickel nitrate, manganese nitrate was dissolved in deionized water with stirring, and then a solution of ammonium carbonate was added dropwise as precipitant. The molar quantity of ammonium carbonate was equal to the sum of nickel and manganese. Then the mixture was filtered after aging for 1 h. The powder was dried in the air at 120 °C for 12 h and then calcined in air at a desired temperature for 6 h. The catalyst was denoted as Ni(x)-MnO_x, x represents the mole ratio of Ni/Mn. MnO_x and NiO_x were prepared by the same method.

2.2. Catalyst characterization

X-ray diffraction patterns were obtained by a Brucker-D8 Advance X-ray diffractometer using CuK_α radiation (40 kV and 40 mA) with the scanning rate of 6° min^{-1} for detection.

A surface area and pore size analyzer (Quantachrome NOVA 4200e) was used to obtain the surface area and pore characterization of catalysts, which were calculated by using the Brunauer–Emmett–Teller (BET) and Barrett–Joyner–Halenda (BJH) methods, respectively. Prior to analysis, 120–200 mg of the sample was degassed in vacuum at 120 °C for 6 h.

X-ray photoelectron spectroscopy (XPS) analyses were carried out on a K-Alpha spectrometer using Al Kα (1486.7 eV) radiation as the excitation source. Sample charging effects were eliminated by correcting the observed spectra with the C 1s binding energy value of 284.6 eV.

The acidic property was obtained by temperature programmed desorption of ammonia (NH_3-TPD). Prior to analysis, 100 mg sample was pretreated in a He stream (30 mL min^{-1}). After that, the sample was saturated with NH_3 (30 mL min^{-1}, 4% in He) for 1 h. The sample was flushed with 30 mL min^{-1} of He for 2 h to remove the weakly bound (physisorbed) NH_3, after which the sample temperature was lowered to 50 °C. Finally, the temperature was ramped to 400 °C at a rate of 10 °C min^{-1}.

Pyridine-IR was performed with a Frontier FTIR spectrophotometer from 1200 to 2000 cm^{-1}. Each time, 10 mg of the sample was grounded into fine powder and pressed into very thin self-supporting wafers with a diameter of 13 mm. Prior to adsorption, the samples were pretreated in situ at 350 °C for 1 h under evacuation with the residual pressure of 1.0×10^{-2} Pa; after cooled to 30 °C, the background spectrum was collected. Pyridine adsorption was performed at 150 °C until the intensity of the spectra no longer changed. The physically adsorbed pyridine was removed by evacuation for 0.5 h. After the sample was heated to 150 °C in vacuum, the pyridine-IR spectra were recorded.

The temperature-programmed reduction (H_2-TPR) experiments were performed on an automated catalyst characterization system (Chemisorb 2750, Micrometrics Company). A gas flow of 25 mL min^{-1} (10% H_2 in Ar) was passed over about 50 mg sample in a quartz reactor. The reduction temperature was linearly raised from 25 °C to 800 °C at a rate of 10 °C min^{-1}.

2.3. Catalytic activity experiments

The low-temperature reduction of NO by ammonia with excess oxygen activity measurements was carried out in a fixed-bed. 200 mg catalyst was placed in the reactor until the NO gas reached the expected equilibrium concentration to ensure that the later decrease in NO concentration was caused by the SCR by ammonia instead of by the adsorption by the catalyst. The reaction gas mixture normally consisted of 550 ppm NO, 550 ppm NH_3, 5% O_2, and N_2 in balance. Under ambient conditions, the total flow rate was 250 mL min^{-1} and the gas hourly space velocity (GHSV) was 64,000 h^{-1}. Reactant and product contents were collected after a steady state was achieved (30–40 min) at the given temperature.

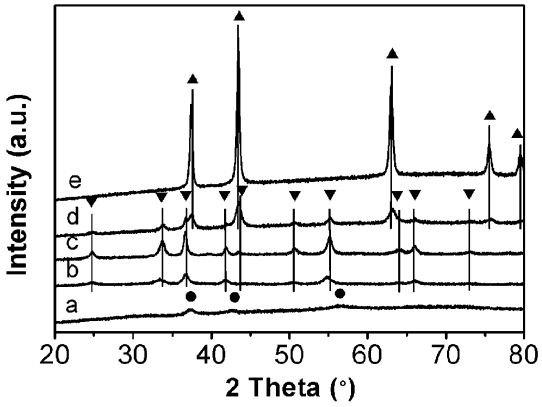

Fig. 1. XRD patterns of (a) MnO_x, (b) Ni(0.4)-MnO_x, (c) Ni(1)-MnO_x, (d) Ni(2.5)-MnO_x and (e) NiO_x calcined at 400 °C, (▲ NiO, ▼ $NiMnO_3$ and ● MnO_2).

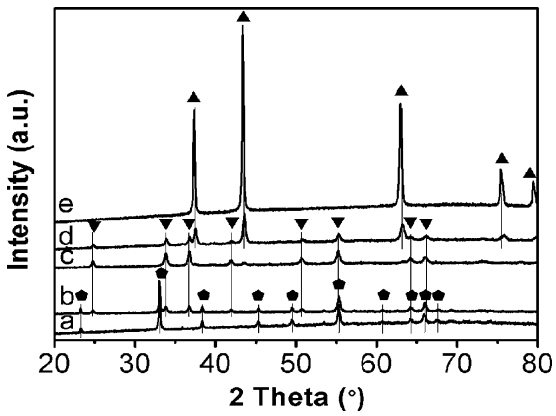

Fig. 2. XRD patterns of (a) MnO_x, (b) Ni(0.4)-MnO_x, (c) Ni(1)-MnO_x, (d) Ni(2.5)-MnO_x and (e) NiO_x calcined at 500 °C, (▲ NiO, ▼ $NiMnO_3$ and ⬟ Mn_2O_3).

NO conversion and N_2 selectivity was calculated as the following equation:

$$\text{NO conversion}\,(\%) = \frac{[NO]_{in} - [NO]_{out}}{[NO]_{in}} \times 100\%,$$

where the subscripts 'in' and 'out' indicate the inlet and outlet concentration at steady state, respectively.

$$N_2\ \text{selectivity}\,(\%) = \frac{[NO]_{in} + [NH_3]_{in} - [NO_2]_{out} - 2[N_2O]}{[NO]_{in} + [NH_3]_{in}} \times 100\%$$

Table 1
Surface area and pore characterization of the catalysts with different Ni/Mn atomic ratios calcined at 400 °C.

Samples	BET surface area ($m^2\ g^{-1}$)	Average pore diameter (nm)	Pore volume ($cm^3\ g^{-1}$)
MnO_x	66.5	33.4	0.26
Ni(0.4)-MnO_x	90.5	12.9	0.25
Ni(1)-MnO_x	15.8	2.8	0.08
Ni(2.5)-MnO_x	29.5	24.2	0.16
NiO_x	17.4	15.3	0.08

3. Results

3.1. XRD analysis

Fig. 1 shows the XRD patterns of the MnO_x, Ni(0.4)-MnO_x, Ni(1)-MnO_x, Ni(2.5)-MnO_x and NiO_x catalysts calcined at 400 °C. The MnO_x sample (Fig. 1a) is basically amorphous with three very broadened and weak peaks of MnO_2 (PDF card 30-0820) with low crystallinity at the temperature. By co-precipitation of nickel and manganese salts at the molar ratios of Ni/Mn at 1:2.5 and 1:1, a Ni-Mn bi-metal oxide phase, $NiMnO_3$ (PDF card 65-3695), can be observed clearly (Fig. 1b and c), however, the diffraction peaks are rather weak, most probably indicating the presence of a large amount of amorphous manganese oxide phase in the samples, especially in Ni(0.4)-MnO_x. When the Ni/Mn molar ratio reaches 2.5:1, a group of sharp peaks of NiO (PDF card 65-5745) phase appears simultaneously with the $NiMnO_3$ phase in the Ni(2.5)-MnO_x catalyst (Fig. 1d).

When the calcination temperature was raised to 500 °C, only Mn_2O_3 (PDF card 41-1442) could be observed in 500 °C calcined MnO_x catalyst (Fig. 2a), indicating that the amorphous manganese oxide in 400 °C calcined MnO_x has mainly crystallized into Mn_2O_3 instead of MnO_2. The Ni(0.4)-MnO_x catalyst after calcination at 500 °C is composed of mixed phases of Mn_2O_3 and $NiMnO_3$ (Fig. 2b), as compared to the single crystalline phase of $NiMnO_3$ in the 400 °C calcined counterpart (Fig. 1b). In addition, the Ni(1)-MnO_x, Ni(2.5)-MnO_x and NiO_x catalysts still remained the same phases (Fig. 2c–e) at the elevated temperature of calcination.

In addition, the amorphous manganese oxide usually showed higher surface areas than the crystallized ones. The surface areas of MnO_x and Ni(0.4)-MnO_x, which contains amorphous manganese oxide phase, are much higher than those of Ni(1)-MnO_x, Ni(2.5)-MnO_x and NiO_x (Table 1), in accordance with the SCR activity results (Fig. 4). Therefore, it can be proposed that the presence of amorphous manganese oxide phase in the MnO_x and Ni(0.4)-MnO_x catalysts may be one of the key factors for their excellent catalytic

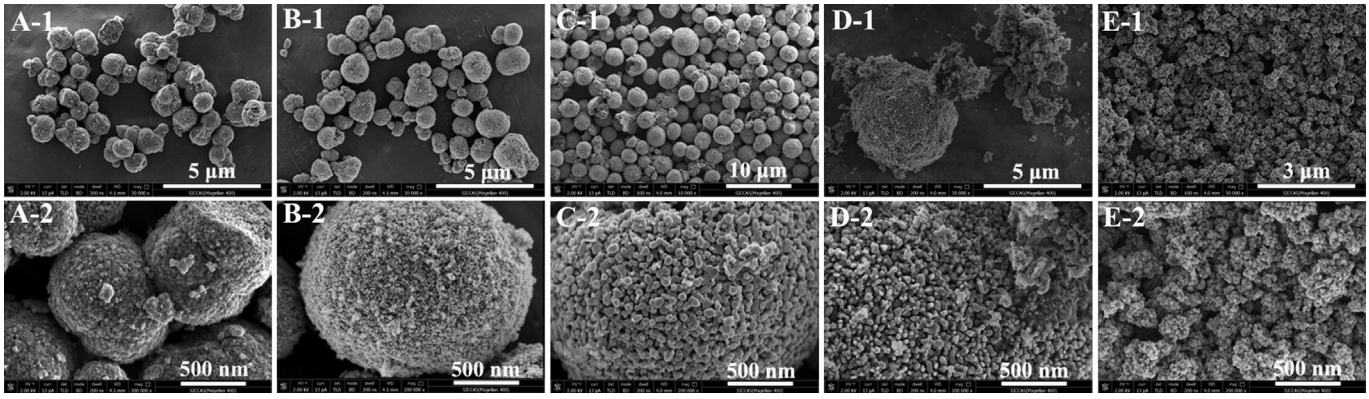

Fig. 3. SEM images of (A) MnO_x, (B) Ni(0.4)-MnO_x, (C) Ni(1)-MnO_x, (D) Ni(2.5)-MnO_x and (E) NiO_x calcined at 400 °C.

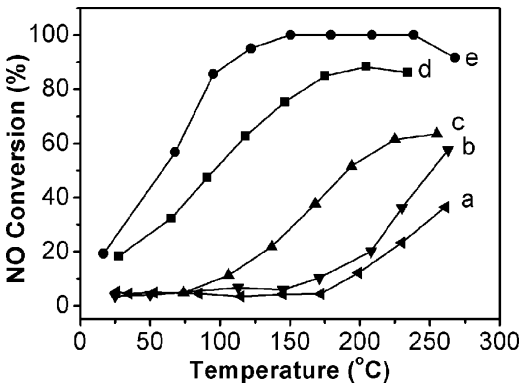

Fig. 4. SCR activity of (a) NiO_x, (b) Ni(2.5)-MnO_x, (c) Ni(1)-MnO_x, (d) MnO_x and (e) Ni(0.4)-MnO_x calcined at 400 °C.
Reaction conditions: [NO] = 500 ppm, [NH_3] = 500 ppm, [O_2] = 5%, GHSV = 64,000 h^{-1}.

activity in agreement with the previous reports by Tang et al. [14] and Kang et al. [15]

3.2. SEM analysis

The SEM images of the catalysts (Fig. 3) clearly reveal the morphology changes with the increase of the nickel content. The MnO_x catalyst shows an aggregated spherical morphology and each aggregate is composed of numbers of irregular small particles corresponding to the amorphous manganese oxide phase (Fig. 3A). With the addition of nickel in Ni(0.4)-MnO_x, the morphology does not changed substantially, however the particles in each spherical aggregate become much smaller (Fig. 3B). When the Ni/Mn ratio reaches 1:1 (Fig. 3C), the spherical aggregates become much more uniform in morphology and dimension, and are composed of particles with enlarged diameters of about 50–70 nm, which agreed with that the intensified XRD peaks of Ni(1)-MnO_x as compared to that of Ni(0.4)-MnO_x. The spherical aggregates become fragmented at increased Ni content, and no aggregate spheres can be found in NiO_x (Fig. 3C–E), which can be associated with the varied phase structures of different samples.

3.3. Low-temperature catalytic performance

Fig. 4 shows the performances of the MnO_x, Ni(0.4)-MnO_x, Ni(1)-MnO_x, Ni(2.5)-MnO_x and NiO_x catalysts calcined at 400 °C for NO SCR with NH_3 in the presence of excess oxygen at the space velocity of 64,000 h^{-1}. The MnO_x catalyst exhibited a relatively well-defined catalytic activity, which matches well with the previous reports [6,11,14,15]. Although the pure NiO_x catalyst showed negligible activity, the Ni(0.4)-MnO_x catalyst performed an excellent catalytic activity which achieved 85% conversion of NO at 95 °C and almost 100% conversion in the range of 150 °C to 240 °C, much higher than the pure MnO_x catalyst. However, with the continuous increase of the molar ratio of Ni/Mn, the catalytic activity decreased dramatically. For the diversification of the product, it is necessary to consider the product selectivity of the catalysts from a greenhouse gas perspective. We evaluated the N_2 selectivity of all catalysts at 120 °C. It can be seen from Fig. 5 that the N_2 selectivity increases from 60% to100% at 120 °C with the increase of Ni/Mn atomic ratio from 0 to 2.5, indicating that the nickel loading has a strong influence on N_2 selectivity.

3.4. Effect of calcination temperature

The calcination temperature has a great effect on the crystallization as well as specific surface area of the catalyst, which are

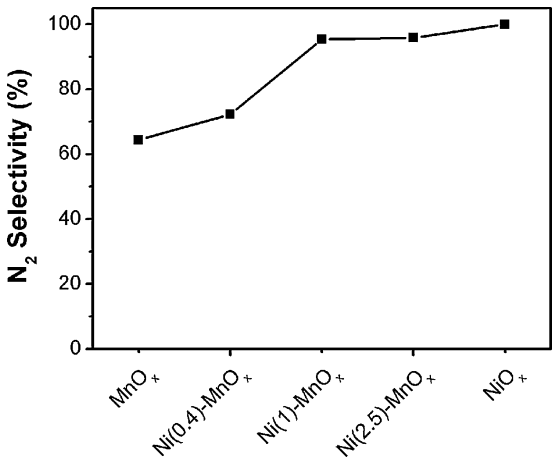

Fig. 5. N_2 selectivity in the SCR reaction over catalysts calcined at 400 °C.
Reaction conditions: [NO] = 500 ppm, [NH_3] = 500 ppm, [O_2] = 5%, GHSV = 64,000 h^{-1}.

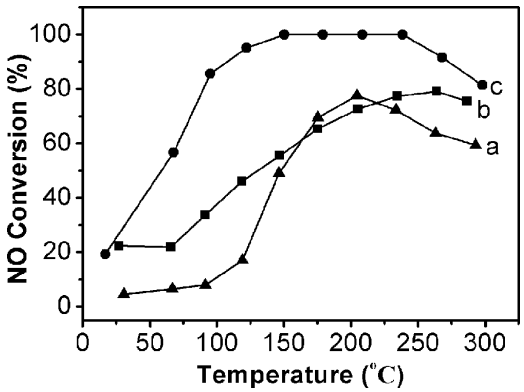

Fig. 6. SCR activity of the Ni(0.4)-MnO_x catalyst calcined at different temperatures: (a) 500 °C, (b) 300 °C, (c) 400 °C. Reaction conditions: [NO] = 500 ppm, [NH_3] = 500 ppm, [O_2] = 5%, GHSV = 64,000 h^{-1}.

critical to the SCR activity of the catalyst [16]. Fig. 6 shows the NO conversion for the Ni(0.4)-MnO_x catalyst calcined at different temperatures. The catalyst calcined at 400 °C gave the optimal SCR activity at low temperatures. Either increasing (500 °C) or decreasing (300 °C) the calcination temperature will lead to the dramatically decreased activity, especially at the elevated temperature.

Fig. 7 presents the XRD patterns of Ni(0.4)-MnO_x calcined at different temperatures. It is clear that the intensities of the XRD peaks

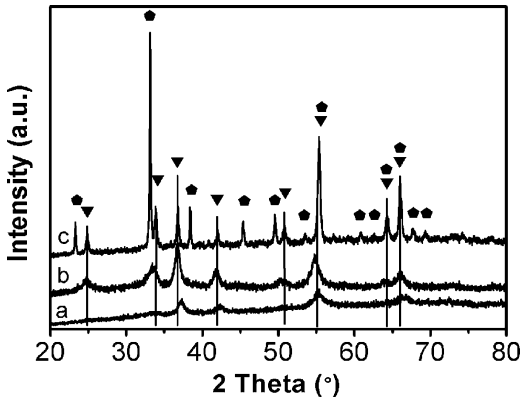

Fig. 7. XRD patterns of the Ni(0.4)-MnO_x catalyst calcined at different temperatures: (a) 300 °C, (b) 400 °C, (c) 500 °C, (▼ $NiMnO_3$, ⬟ Mn_2O_3).

Table 2
Surface area and pore characterization of the Ni(0.4)-MnO_x catalyst calcined at different temperatures.

Samples	BET surface area ($m^2\ g^{-1}$)	Average pore diameter (nm)	Pore volume ($cm^3\ g^{-1}$)
Ni(0.4) -MnO_x (300 °C)	87.2	12.9	0.23
Ni(0.4)-MnO_x (400 °C)	90.5	12.9	0.25
Ni(0.4)-MnO_x (500 °C)	13.3	1.9	0.02

get much sharper with the increasing calcination temperature, implying that the ever complete crystallization and the substantial crystallite growth of the catalysts when the calcination temperature was raised from 300 °C to 500 °C.

The BET surface area, pore volume and pore size of the Ni(0.4)-MnO_x catalyst calcined at different temperatures are summarized in Table 2. It can be found that the BET surface areas of Ni(0.4)-MnO_x calcined at 300 °C and 400 °C are much higher than that of Ni(0.4)-MnO_x calcined at 500 °C, which might be attributed to the existence of the amorphous manganese oxide phase and/or the incompleteness of crystallization. It has been widely known that the surface area is not the only parameter affecting the activity, the chemical composition, the phase structure and particle crystallization might be more predominant in many cases. For example, the poor SCR activity of the catalyst calcined at 300 °C might be ascribed to the low crystallinity though it has a relatively high surface area. Therefore, various factors such as surface area, chemical and phase composition, and crystallization will co-affect the SCR activity, which result in the final dependence of the SCR activity on calcination temperature.

3.5. Lifetime study, H_2O and SO_2 tolerance of the Ni(0.4)-MnO_x catalyst

As reported above, the Ni(0.4)-MnO_x catalyst calcined at 400 °C demonstrated the highest SCR activity. Its lifetime and regeneration properties were then investigated. Fig. 8 gives the NO conversions in the time course over 100 h at 230 °C on the 400 °C calcined Ni(0.4)-MnO_x catalyst. The test results demonstrated that during the first 10 h, the SCR activity maintained a very high NO conversion at 100% and still remained at 95.4% after a 100 h continuous lifetime test. After turning off the total reaction gas stream for 10 h, the NO conversion was recovered to 100% without any external treatment on the catalyst. These results indicate that the Ni(0.4)-MnO_x catalyst possesses a satisfactorily high stability and self-regeneration capability as a catalyst for NO SCR.

It is also important to evaluate the water affect on the catalyst. Fig. 9 illustrates the H_2O tolerance of the Ni(0.4)-MnO_x catalyst to

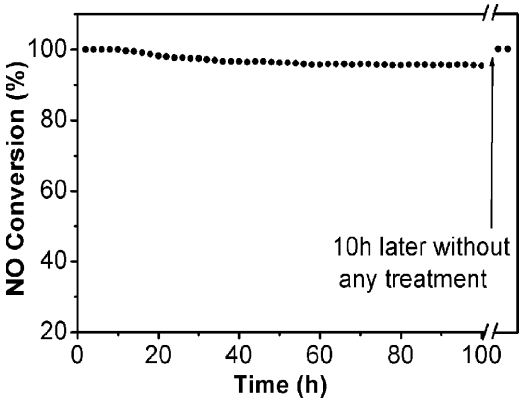

Fig. 8. Lifetime study of the Ni(0.4)-MnO_x catalyst at 230 °C.
Reaction conditions: [NO] = 500 ppm, [NH_3] = 500 ppm, [O_2] = 5%, [SO_2] = 100 ppm, GHSV = 64,000 h^{-1}.

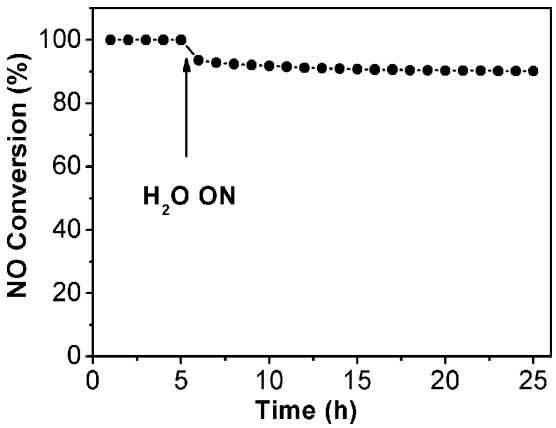

Fig. 9. Influence of water on NO conversion in the SCR reaction over Ni(0.4)-MnO_x catalyst at 230 °C. Reaction conditions: [NO] = 500 ppm, [NH_3] = 500 ppm, [O_2] = 5%, [H_2O] = 10%, GHSV = 64,000 h^{-1}.

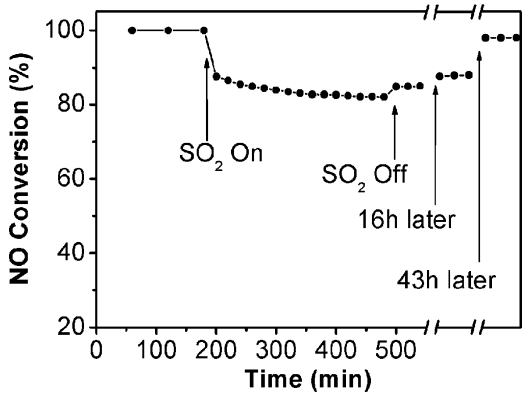

Fig. 10. SO_2-tolerance study of the Ni(0.4)-MnO_x catalyst at 230 °C.
Reaction conditions: [NO] = 500 ppm, [NH_3] = 500 ppm, [O_2] = 5%, [SO_2] = 100 ppm, GHSV = 64,000 h^{-1}.

steam poisoning for 20 h during the SCR of NO with NH_3 at 230 °C. We carried out the SCR of NO reaction with high gas hourly space velocity (GHSV) 64,000 h^{-1} in the presence of 10 vol.% H_2O. The NO conversion decreased to 93.6% from 100% when H_2O of 10% was added and maintained at 90% in the following 20 h. This result indicated that the Ni(0.4)-MnO_x catalyst displays a good H_2O tolerance.

Industrially, a certain amount of SO_2, usually about 100 ppm, may still exist after a desulphurization process. Thus it is necessary to evaluate the SO_2 tolerance of the catalyst. Fig. 10 shows the SCR activity over the Ni(0.4)-MnO_x catalyst in the presence of SO_2 (100 ppm) at 230 °C under a space velocity of 64000 h^{-1}. When the SO_2 was added to the reaction gas stream, the NO conversion decreased from 100% to 87% and still remained at 82% in 5 h. When the SO_2 flow was stopped, the NO conversion increased to 85%. After stopping the total reaction gas stream for 16 h, the NO conversion of the catalyst recovered to 88% and finally to 98% after a 43-h stopping without any additional treatment. Although the Ni(0.4)-MnO_x catalyst displays a relatively good stability, H_2O and SO_2 tolerance in our small-scale lab, the long-term and large-scale sulfur-tolerance properties of the catalyst need to be further investigated.

4. Discussion

4.1. H_2-TPR analysis

The H_2-TPR of the pure MnO_x, Ni(0.4)-MnO_x and Ni(1)-MnO_x catalysts calcined at 400 °C were carried out and evaluated for

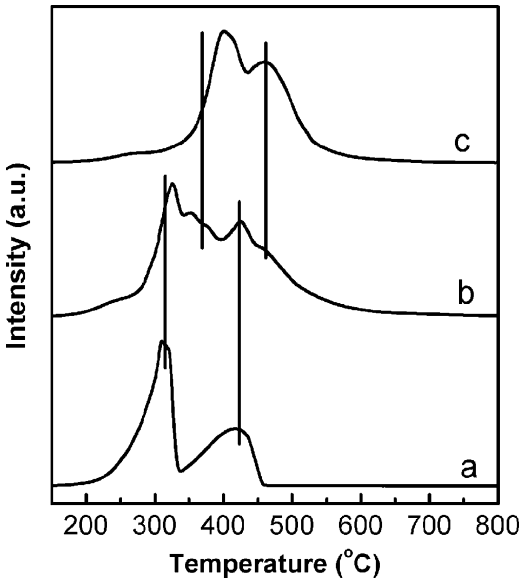

Fig. 11. H_2-TPR patterns of (a) MnO_x, (b) Ni(0.4)-MnO_x and (c) Ni(1)-MnO_x calcined at 400 °C.

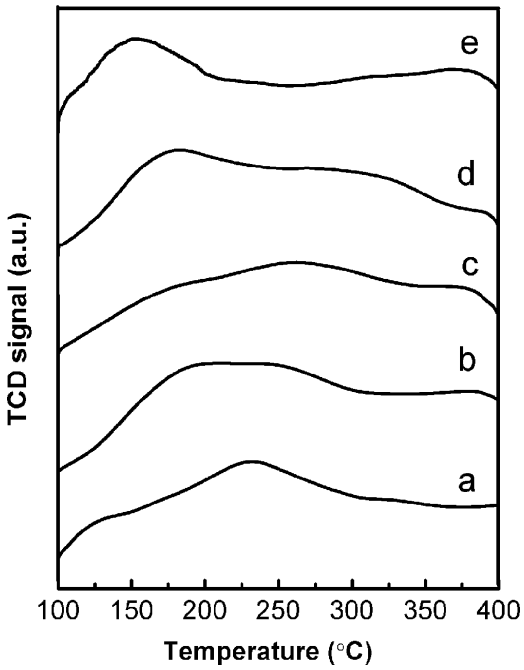

Fig. 12. NH_3-TPD patterns of (a) MnO_x, (b) Ni(0.4)-MnO_x, (c) Ni(1)-MnO_x, (d) Ni(2.5)-MnO_x and (e) NiO_x calcined at 400 °C.

understanding the SCR reaction (Fig. 11). The profile of the pure MnO_x catalyst showed two reduction peaks at 315 °C and 426 °C (Fig. 11a). According to the XRD result, the 400 °C calcined MnO_x catalyst composed of a main amorphous manganese oxide phase and small amount of MnO_2 phase, the reduction peaks at 315 °C and 426 °C can be associated to the two-step reductions of MnO_2 via Mn_2O_3/Mn_3O_4 to MnO, in good agreement with the previous studies that the reduction of bulk MnO_2 and/or Mn_2O_3 takes place through a distinct two-step reduction process [12,17–20]. Further reduction of MnO to Mn metal is impossible below 800 °C due to its large negative value of reduction potential, which had been reported by many studies [12,20–22]. The H_2-TPR profile of Ni(1)-MnO_x gives two overlapped strong reduction peaks at 398 °C and 461 °C (Fig. 11c), which can be assigned to the two reduction steps of $NiMnO_3$: Mn^{4+} to Mn^{3+} and Mn^{3+} to Mn^{2+} [12,20,23,24], considering that $NiMnO_3$ is the only phase in Ni(1)-MnO_x (see the sections of XRD analysis). The H_2-TPR pattern of Ni(0.4)-MnO_x was characterized by two distinct reduction peaks at 326 and 425 °C, and two slight shoulders at 354–380 °C and 450–500 °C (Fig. 11b), a combination of the TPR patterns of MnO_x and Ni(1)-MnO_x, which again indicates the Ni(0.4)-MnO_x catalyst is a mixture of amorphous manganese oxides and $NiMnO_3$ (Fig. 2b). Thus, the two reduction peaks at 326 °C and 425 °C for the Ni(0.4)-MnO_x catalyst can be ascribed to the reductions of the amorphous manganese oxides, meanwhile the two slight reduction shoulders represent the reductions of $NiMnO_3$ phase [12,20,23,24]. In spite of these, it can be found that the reduction peaks at 326 °C and 425 °C shifted to higher temperatures compared with those of the pure MnO_x catalyst and the two weak reduction shoulders at 354–380 °C and 450–500 °C shifted to lower temperatures compared with those of Ni(1)-MnO_x. Meanwhile the amount of H_2 consumed at 326 °C (136.3 mL g^{-1}) of Ni(0.4)-MnO_x is much greater than that of MnO_x (84.2 mL g^{-1}), implying that the reducing potential of Ni(0.4)-MnO_x should be significantly higher than that of MnO_x [12]. Both the position shifts of the reduction peaks and the difference in the consumed H_2 amounts between Ni(0.4)-MnO_x and MnO_x indicate that an interaction must have taken place between the phases (amorphous manganese oxides and $NiMnO_3$) in the Ni(0.4)-MnO_x catalyst [12,23], which might be important in the synergetic SCR of NO. Additionally, the first reduction peaks of both MnO_x and Ni(0.4)-MnO_x located at much lower temperatures than that of Ni(1)-MnO_x, implying their reduction potentials in the low temperatures should be much higher than that of Ni(1)-MnO_x [25], which should be an important reason for their excellent low temperature SCR activities [26]. Because the first peaks of MnO_x and Ni(0.4)-MnO_x refer to the reduction of Mn^{4+} to Mn^{3+} regardless in the forms of MnO_2, amorphous manganese oxides or $NiMnO_3$ in the catalysts, it can be proposed that the excellent low temperature SCR activities should be related with the reduction of Mn^{4+} to Mn^{3+}, which will be further discussed in the following XPS section.

4.2. NH_3-TPD and in situ FT-IR analysis

It is well known that the surface acidity of catalyst always plays an important role in the low temperature SCR of NO by NH_3 [4]. Therefore, the NH_3-TPD was carried out to evaluate the acid site distribution of the prepared catalysts (Fig. 12). The desorption peak of the MnO_x catalyst at the temperature range of 150–300 °C is usually attributed to the NH_3 desorption from weak and medium acid sites distributed on the surface of catalysts [27,28]. In the cases of Ni(0.4)-MnO_x, Ni(1)-MnO_x and Ni(2.5)-MnO_x, the broadened desorption peak and enhanced chemisorbed NH_3 amounts, especially at temperature range of 120–250 °C, were recorded, which suggests that the addition of nickel has remarkably enhanced the concentration and acidity of acid sites [17,29]. For the Ni(2.5)-MnO_x and NiO_x catalysts, the distinct peak at 150–180 °C should be attributed to the NH_3 desorption from the acid sites of nickel oxide phase.

In order to better understand the nature of the acid sites and the role of the nickel addition, in situ FT-IR experiments on MnO_x and Ni(0.4)-MnO_x were performed. Fig. 13 shows the adsorption and desorption characteristics of pyridine over the MnO_x and Ni(0.4)-MnO_x catalysts in a wavenumber range of 1200–2000 cm^{-1}. In both cases, compared to the framework figures, two peaks around 1450 and 1590 cm^{-1} appeared after pyridine adsorption at 30 °C, suggesting the presence of Lewis acid sites on the surface of the MnO_x and Ni(0.4)-MnO_x catalysts and the absence of apparent Brönsted acid sites (1540 cm^{-1}) [30–34]. After desorption at 150 °C,

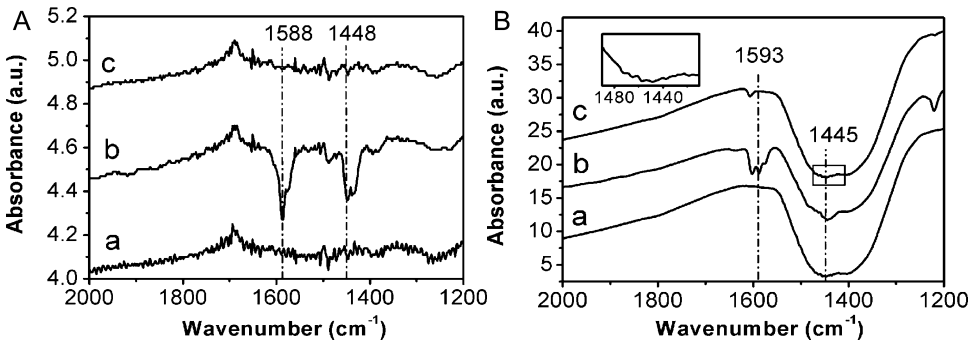

Fig. 13. In situ FT-IR spectra of adsorbed pyridine over (A) MnO_x and (B) Ni(0.4)-MnO_x. (a) framework, (b) adsorption at 30 °C and (c) desorption at 150 °C.

Table 3
Acid strength distribution of the MnO_x and Ni(0.4)-MnO_x catalysts.

Sample	Absorption (cm^{-1})	Acid amount (mmol g^{-1})
MnO_x	1448	0.02
	1588	0.03
Ni(0.4)-MnO_x	1445	0.06
	1593	0.11

the disappearance of the above two absorption peaks indicates that the Lewis acid sites distributed on the surface were relatively weak in agreement with the TPD results. Table 3 shows that Ni(0.4)-MnO_x has a larger amount of Lewis acid sites than MnO_x at both 1450 cm^{-1} and 1590 cm^{-1}, strongly supporting the results of TPD and the previous reports [1,29,35] that the addition of nickel can increase the concentration and acidity of Lewis acid sites on the surface of the Ni(0.4)-MnO_x catalysts.

4.3. XPS analysis and a possible redox reaction over Ni(0.4)-MnO_x

To acquire the information about the oxidation states and the atomic compositions of manganese and nickel cations on the catalyst surface, the XPS spectra of Mn 2p, Ni 2p in the fresh catalysts calcined at 400 °C were recorded (Fig. 14), which had been calibrated against the C ls peak standardized at 284.6 eV [25]. For all samples, two main peaks due to Mn $2p_{3/2}$ and Mn $2p_{1/2}$ can be observed from 641.7 eV to 653.9 eV (Fig. 14A). By performing a peak-fitting deconvolution, the Mn $2p_{3/2}$ spectra were separated into three peaks, Mn^{3+} (641.0–641.3 eV), Mn^{4+} (642.0–642.5 eV) and Mn nitrate (644.2–644.8 eV) [1,3,10,25,36,37]. The Ni $2p_{3/2}$ spectra were separated into two peaks at 854.2–854.4 eV and 856.0–856.2 eV, by the same peak-fitting deconvolution technique (Fig. 14B), assigned to Ni^{2+} and Ni^{3+}, respectively [36–38]. Additionally, another characteristic satellite peak at around 862 eV can be explained as the multiple splitting in the energy level of the Ni-containing oxides which was also observed in NiO, $LiNiO_2$, $Li(Ni_{1/3}Co_{1/3}Mn_{1/3})O_2$, $Li(Ni_{1/2}Mn_{1/2})O_2$ and $Li(Mn_{1.5}Ni_{0.5})O_4$ [36–40].

Table 4 lists the percentages of different valence states of manganese and nickel determined by XPS. It was found that the surface Mn^{4+} was the predominant valence state of manganese and the percentage of Mn^{4+} decreased as following: Ni(0.4)-MnO_x > MnO_x > Ni(1)-MnO_x > Ni(2.5)-MnO_x, exactly the same order as their SCR activities. Considering that the SCR activities of the catalysts should be related to the reduction of Mn^{4+} to Mn^{3+} as discussed in the section of TPR analysis, it can be proposed that Mn^{4+} must have played an important role in the catalytic redox process, in agreement with many previous reports that Mn^{4+} was preferable for oxidation reaction over manganese-containing catalysts [1,3,11–13].

4.4. Synergetic effect between Ni and Mn ions

According to the above results of H_2-TPR, NH_3-TPD, in situ FT-IR and XPS, it was revealed that Mn^{4+} is the main active species for SCR reaction and the addition of nickel enhanced the surface concentration and acidity of Lewis acid sites. However, it was found (Table 4) that the percentages of different valence states of manganese and nickel species on the surface of Ni(0.4)-MnO_x (used) did not change significantly after undergoing SCR reaction for 100 h, compared with those of the fresh catalyst. We therefore propose a possible synergetic catalytic effect (redox cycle) between manganese and nickel ions for low temperature SCR reaction over the

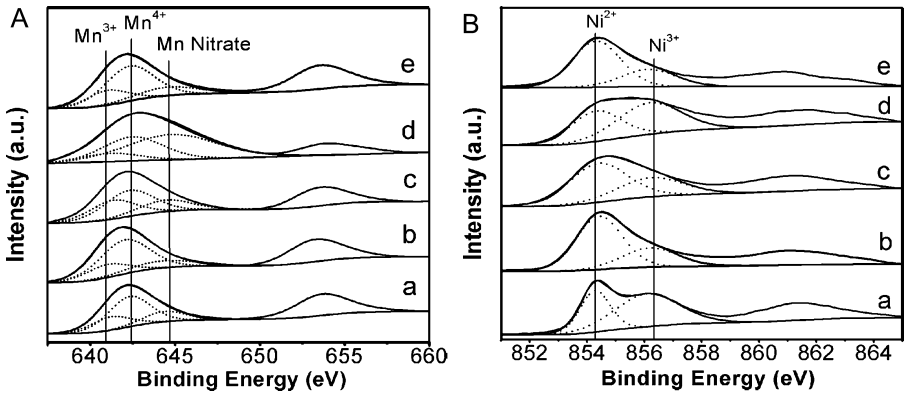

Fig. 14. XPS spectra for A—Mn 2p, B-Ni 2p of the catalysts calcined at 400 °C. A—(a) MnO_x, (b) Ni(0.4)-MnO_x, (c) Ni(1)-MnO_x, (d) Ni(2.5)-MnO_x, (e) Ni(0.4)-MnO_x-used; B—(a) NiO_x, (b) Ni(0.4)-MnO_x, (c) Ni(1)-MnO_x, (d) Ni(2.5)-MnO_x, (e) Ni(0.4)-MnO_x-used.

Table 4
Binding energies and the percent of different valence states for manganese and nickel determined from deconvoluted XPS spectra.

Catalyst	Percent of valence state, % (binding energy, eV)				
	Mn^{3+}	Mn^{4+}	Mn nitrate	Ni^{2+}	Ni^{3+}
MnO_x	23.73(641.2)	56.89(642.3)	19.39(644.4)	–	–
Ni(0.4)-MnO_x	20.67(641.0)	61.98(642.0)	17.35(644.2)	69.74 (854.4)	30.26 (856.2)
Ni(1)-MnO_x	31.39(641.3)	46.63(642.3)	21.98(644.5)	64.60 (854.4)	35.40 (856.2)
Ni(2.5)-MnO_x	11.46(641.2)	34.43(642.5)	54.12(644.8)	43.34 (854.3)	56.66 (856.2)
NiO_x	–	–	–	37.20(854.28)	62.80(856.09)
Ni(0.4)-MnO_x-used	21.32(641.0)	60.41(642.3)	18.27(644.6)	70.18 (854.2)	29.82 (856.0)

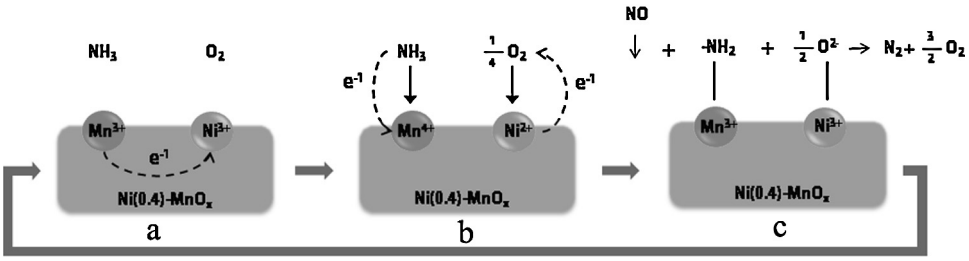

Scheme 1. The proposed mechanism of the SCR reaction over the Ni(0.4)-MnO_x catalyst and the synergetic catalytic effect between Mn and Ni cations. Mn^{3+} is activated by Ni^{3+} into Mn^{4+}, which is responsible for the NH_3 dehydration into–NH_2 and H^+, and the final low temperature NO SCR into N_2 and H_2O in the presence of oxygen.

Ni(0.4)-MnO_x catalyst through the electron transfer between Mn and Ni ions to maintain a dynamic equilibrium, as depicted in Scheme 1. In Scheme 1a, Ni^{3+} captures an electron from Mn^{3+} and they become Ni^{2+} and Mn^{4+}, respectively, such a process is similar as those of $Ni^{4+} + Co^{3+} \leftrightarrow Ni^{3+} + Co^{4+}$ [41], $Fe^{3+} + Ni^{4+} \leftrightarrow Fe^{4+} + Ni^{3+}$ [42], $Cr^{5+} + 2Mn^{3+} \leftrightarrow Cr^{3+} + 2Mn^{4+}$ [2] and $Cu^{2+} + Mn^{3+} \leftrightarrow Cu^{+} + Mn^{4+}$ [9,36]. In this process, Mn^{3+} is actually activated by Ni ion to its activated state of Mn^{4+}, which is responsible for the dehydration of NH_3 to $–NH_2$ (Scheme 1b) [3], and finally for the NO SCR, and can thus be classified as a type I of synergetic effect as recently proposed by Shi [43]. This synergetic effect contributed to the enhanced NO SCR activity and the high stability and self-regeneration property of the Ni(0.4)-MnO_x catalyst as well (Fig. 8). In the meantime Ni^{3+} is actually mutually activated into Ni^{2+} by the electron transfer via $Mn^{3+} + Ni^{3+} \leftrightarrow Mn^{4+} + Ni^{2+}$, the generated Ni^{2+} will reduce O_2 into O^{2-}, by donating an electron to O_2 (Scheme 1b), and simultaneously changes back to Ni^{3+}. Finally $–NH_2$ and O^{2-} reacted with gas NO and generated N_2 and H_2O (Scheme 1c). The catalytic reaction continues following the next cycle of Mn ion activation by $Mn^{3+} + Ni^{3+} \leftrightarrow Mn^{4+} + Ni^{2+}$.

5. Conclusions

A series of Ni-Mn bi-metal oxide catalysts with high activity for the low temperature selective catalytic reduction (SCR) of NO with NH_3 in the presence of excess O_2 have been prepared by co-precipitation method with various molar ratios of Ni/Mn. The Ni(0.4)-MnO_x catalyst offered the best catalytic activity, which obtained 85% of NO conversion at 95 °C and 100% from 150 °C to 250 °C under flow conditions of GHSV = 64,000 h^{-1}. The Ni(0.4)-MnO_x catalyst is found to be a mixture of $NiMnO_3$ and amorphous manganese oxide from the XRD patterns. TPR, NH_3-TPD, in situ FTIR and XPS results revealed that Mn^{4+} is the main active species for SCR reaction and the addition of nickel enhanced the surface concentration and acidity of Lewis acid sites. A possible redox cycle-based synergetic catalytic effect has been proposed for low temperature SCR reaction over the Ni(0.4)-MnO_x catalyst through the electron transfer between Mn and Ni ions, which is also believed to be responsible for the self-regeneration capability of the catalyst.

Acknowledgment

This study was financially supported by the National Key Basic Research Program of China (973 Program) (Grant No. 2013CB933200), the National Natural Science Foundation of China (Grant Nos. 21001043, 21073059 and 51372084), the Fundamental Research Funds for the Central Universities (222201313010) and the Nano-Special Foundation for Shanghai Committee of Science and Technology (12nm0502600).

References

[1] T. Bonigari, P.G. Smirniotis, J. Catal. 288 (2012) 74–83.
[2] Z. Chen, Q. Yang, H. Li, X. Li, L. Wang, S. Chi Tsang, J. Catal. 276 (2010) 56–65.
[3] S. Yang, C. Wang, J. Li, N. Yan, L. Ma, H. Chang, Appl. Catal., B: Environ. 110 (2011) 71–80.
[4] Z. Wu, B. Jiang, Y. Liu, Appl. Catal., B: Environ. 79 (2008) 347–355.
[5] G. Qi, R.T. Yang, Appl. Catal., B: Environ. 44 (2003) 217–225.
[6] M. Kang, E.D. Park, J.M. Kim, J.E. Yie, Appl. Catal. A. 327 (2007) 261–269.
[7] S.I. Yi, Y. Liang, S. Thevuthasan, S.A. Chambers, Surf. Sci. 443 (1999) 212–220.
[8] G. Qi, R.T. Yang, R. Chang, Appl. Catal., B: Environ. 51 (2004) 93–106.
[9] M. Kang, E.D. Park, J.M. Kim, J.E. Yie, Catal. Today 111 (2006) 236–241.
[10] D.A. Pena, B.S. Uphade, P.G. Smirniotis, J. Catal. 221 (2004) 421–431.
[11] F. Kapteijn, L. Singoredjo, A. Andreini, J. Moulijn, Appl. Catal., B: Environ. 3 (1994) 173–189.
[12] X. Tang, Y. Li, X. Huang, Y. Xu, H. Zhu, J. Wang, W. Shen, Appl. Catal., B: Environ. 62 (2006) 265–273.
[13] S.M. Lee, K.H. Park, S.S. Kim, D.W. Kwon, S.C. Hong, J. Air. Waste Manage. 62 (2012) 1085–1092.
[14] X. Tang, J. Hao, W. Xu, J. Li, Catal. Commun. 8 (2007) 329–334.
[15] M. Kang, T.H. Yeon, E.D. Park, J.E. Yie, J.M. Kim, Catal. Lett. 106 (2006) 77–80.
[16] J. Huang, Z. Tong, Y. Huang, J. Zhang, Appl. Catal., B: Environ. 78 (2008) 309–314.
[17] P.M. Sreekanth, P.G. Smirniotis, Catal. Lett. 122 (2008) 37–42.
[18] B. Thirupathi, P.G. Smirniotis, Catal. Lett. 141 (2011) 1399–1404.
[19] M. Richter, A. Trunschke, U. Bentrup, K.W. Brzezinka, E. Schreier, M. Schneider, M.M. Pohl, R. Fricke, J. Catal. 206 (2002) 98–113.
[20] J. Trawczyński, B. Bielak, W. Miśta, Appl. Catal. B: Environ. 55 (2005) 277–285.
[21] F. Buciuman, F. Patcas, T. Hahn, Chem. Eng. Process. 38 (1999) 563–569.
[22] J. Carnö, M. Ferrandon, E. Björnbom, S. Järås, Appl. Catal., A. 155 (1997) 265–281.
[23] P.M. Sreekanth, D.A. Peña, P.G. Smirniotis, Ind. Eng. Chem. Res. 45 (2006) 6444–6449.
[24] S. Ponce, M. Pena, J. Fierro, Appl. Catal., B: Environ. 24 (2000) 193–205.
[25] B. Thirupathi, P.G. Smirniotis, Appl. Catal., B: Environ. 110 (2011) 195–206.
[26] S.M. Saqer, D.I. Kondarides, X.E. Verykios, Appl. Catal., B: Environ. 103 (2011) 275–286.
[27] Z. Wu, R. Jin, Y. Liu, H. Wang, Catal. Commun. 9 (2008) 2217–2220.
[28] R. Jin, Y. Liu, Z. Wu, H. Wang, T. Gu, Chemosphere 78 (2010) 1160–1166.
[29] Z. Si, D. Weng, X. Wu, J. Yang, B. Wang, Catal. Commun. 11 (2010) 1045–1048.
[30] C. Bilgiç, Surf. Interface. Anal 42 (2010) 959–962.

[31] T. Barzetti, E. Selli, D. Moscotti, L. Forni, J. Chem. Soc., Faraday Trans. 92 (1996) 1401–1407.
[32] M. Mhamdi, S. Khaddar-Zine, A. Ghorbel, Appl. Catal. A. 357 (2009) 42–50.
[33] M. Meng, L. Guo, J. He, Y. Lai, Z. Li, X. Li, Catal. Today 175 (2011) 72–77.
[34] Y. Liu, T. Gu, Y. Wang, X. Weng, Z. Wu, Catal. Commun. 18 (2012) 106–109.
[35] R. Erdogan, O. Ozbek, I. Onal, Surf. Sci. 604 (2010) 1029–1033.
[36] K. Shaju, G. Subba Rao, B. Chowdari, Electrochim. Acta 48 (2002) 145–151.
[37] K. Shaju, G. Subba Rao, B. Chowdari, Electrochim. Acta 48 (2003) 1505–1514.
[38] A. Carley, S. Jackson, J. O'shea, M. Roberts, Surf. Sci. 440 (1999) L868–L874.
[39] K. Amine, H. Tukamoto, H. Yasuda, Y. Fujita, J. Electrochem. Soc. 143 (1996) 1607–1613.
[40] A. Mansour, Surf. Sci. Spectra 3 (1994) 279–286.
[41] D. Carlier, M. Ménétrier, C. Grey, C. Delmas, G. Ceder, Phys. Rev. B 67 (2003) 174103.
[42] G. Prado, A. Rougier, L. Fournes, C. Delmas, J. Electrochem. Soc. 147 (2000) 2880–2887.
[43] J. Shi, Chem. Rev. 113 (2013) 2139–2181.